DHAFGan: A Dense Hybrid Attention Fusion Generative Adversarial Network for Infrared and Visible Image Fusion

Qiong Hong[a,*], Zhonghua Xu[b], Dongli Qin[c], Yuhui Zheng[d] and Hao Zhang[b]

[a] Business School, Jiangsu Vocational College of Electronics and Information, Huaian 223003, China.

[b] School of Transportation Engineering, Huai'an University, Huaian 223003,China.

[c] Smart Campus Service Center, Jiangsu Vocational College of Finance and Economics, Huai'an 223003, China.

[d] School of Artificial Intelligence, Nanjing University of Information Science and Technology, Nanjing, 210044, China.

Abstract: Aiming at the problems existing in the current infrared and visible light image fusion algorithms, such as insufficient perception of typical features, poor visual representation of the fusion results, and insufficient utilization of important secondary information, this paper proposes an infrared and visible light image fusion algorithm based on shallow-deep feature extraction and dual-channel hybrid attention. Firstly, a shallow-deep feature extraction module is constructed. This module utilizes shallow convolutional layers and deep multi-scale receptive field units to extract surface-level features and deep semantic information from the source images, respectively, thereby achieving multi-level multimodal feature extraction. Secondly, Dual-Channel Hybrid Attention Fusion Module (DCAFM) is constructed. Spatial attention is focused on the salient areas of the image, and channel attention is used to strengthen the feature channels, thereby enhancing the fusion ability of multimodal features. Finally, primary and secondary feature loss functions are formulated to constrain both the generator and discriminator, facilitating the extraction of latent secondary feature information from the source images. Experimental results on the DroneVehicle dataset demonstrate that the proposed algorithm achieves superior performance in both subjective visual evaluation and objective metrics. Quantitative evaluations show that our method outperforms seven state-of-the-art approaches, achieving the highest scores in standard deviation (SD=9.3541), mutual information (MI=2.4321), and peak signal-to-noise ratio (PSNR=65.7852), while ranking second in average gradient

(AG=3.9854). The fused images generated by our method not only align with human visual perception characteristics but also retain rich detailed information, effectively preserving both dominant and subtle features from the source modalities.

Keywords: Image Fusion, Multi-Scale Receptive Field, Dual-Channel Hybrid Attention, Loss Of Primary and Secondary Features

1. Introduction

In the construction of smart cities, IoT devices and image fusion technology can be used in a variety of fields, such as urban traffic management, environmental monitoring, and public safety. By deploying numerous IoT cameras and sensors integrated with image fusion technology, comprehensive urban perception and intelligent management can be achieved.

Since the 1980s, growing demands from fields such as military, public security, and border defense for multimodal image fusion have significantly driven the research and development of infrared and visible image fusion technologies. A relatively comprehensive technical framework has now been established, yielding a variety of fusion algorithms that have been successfully applied in numerous domains. These algorithms can be broadly categorized into traditional methods and deep learning-based approaches, based on their underlying fusion strategies.

Traditional infrared and visible image fusion algorithms typically follow a three-stage pipeline: image feature extraction, feature fusion, and image reconstruction, which are executed progressively. Depending on the transformation methods employed, traditional approaches primarily include multi-scale decomposition, sparse representation, subspace-based methods, saliency-based techniques, and hybrid algorithms. Fusion algorithms based on multi-scale decomposition are widely used for multimodal images **[1, 2]**. These methods typically involve three steps: first, performing multi-scale decomposition on the source image; second, processing the decomposed features according to specific fusion rules; and finally, reconstructing the fused image through an inverse transformation. Common transformation methods include pyramid transforms, non-subsampled contourlet transforms, and edge-preserving filters, among

others. For instance, Jin et al. [3] developed an improved Laplacian pyramid transform by calculating the ratio between adjacent low-pass filtered images in the Gaussian pyramid, thereby enhancing local contrast information extraction. Zuo et al. [4] decomposed the source image using a region segmentation strategy within the two-tree discrete wavelet transform, enhancing the algorithm's stability and enabling irregular sampling. However, the inherent limitations of two-dimensional wavelet transforms make it difficult to fully capture the rich directional information present in source images. In this regard, Meng et al. [5] employed non-subsampled contourlet transform to achieve multi-directional information extraction and fusion, which better preserves texture details in the resultant image, albeit with some residual visual artifacts. To further mitigate visual artifacts, Ma et al. [6] proposed a fusion method based on Gaussian and rolling guidance filters.. This approach reduces visual artifacts while enhancing the overall visual quality, producing results that align more closely with human visual perception.. However, multi-scale decomposition-based fusion algorithms remain susceptible to deviations in fusion results caused by image registration errors and noise. Further optimization efforts have led to the exploration of sparse representation-based fusion algorithms. These methods have garnered significant attention from researchers worldwide due to their ability to learn dictionaries from large sets of natural images, thereby enhancing image representation. For example, Liu et al. [7] developed an adaptive sparse representation algorithm that replaces traditional fixed dictionaries with sub-dictionaries learned directly from source images. This approach not only reduces visual artifacts in the fused image but also lowers computational costs.. Subspace-based fusion algorithms map high-dimensional image information into lower-dimensional subspaces. This process reduces redundant information while enhancing the generalization capability of the fusion model. Prominent techniques in this category include principal component analysis (PCA) [8-10], independent component analysis (ICA) [11, 12], and non-negative matrix factorization (NMF) [13, 14]. These algorithms typically employ a sliding window technique for image decomposition. Saliency-based fusion algorithms prioritize salient regions and the objects within them. It mainly includes two categories: the calculation of salient feature weights and the extraction of salient features from feature maps. For

instance, Ma et al. [6] significantly enhanced contrast in the fused image by extracting target weights from source images using visual saliency maps. Zhang et al. **[15]** addressed the problem of imbalanced information retention by constructing saliency maps to guide feature fusion. Recognizing the respective advantages of the above-mentioned algorithms, some scholars have comprehensively improved the fusion effect by conducting algorithm fusion. For example, hybrid algorithms integrating multi-scale transformation with saliency detection **[16, 17]** can highlight object information in salient regions while simultaneously preserving detailed texture information.

In recent years, the successful application of deep learning in computer vision and image processing has led to its widespread adoption for image fusion. Deep learning-based methods, which leverage neural networks to autonomously extract features and enhance the adaptability of fusion algorithms, have attracted significant scholarly interest. Pioneering work by Li et al. **[18]** introduced an autoencoder-based framework for feature extraction in image fusion. However, the reliance on L1-norm-based fusion rules limited the performance and adaptability of this approach.Zhang et al. **[19]** enhanced the retention of multimodal image information by incorporating dense connections and multi-scale attention mechanisms into the autoencoder. Liu et al. **[20]** were among the first to integrate convolutional neural networks (CNNs) into the feature fusion stage. Nevertheless, the continued dependence on hand-crafted fusion rules for feature extraction ultimately constrained the fusion performance. To address these limitations, Xu et al. **[21]** proposed an end-to-end fusion algorithm by introducing a consistency measurement loss, which mitigated the challenge of manual weight allocation during fusion. However, the relatively simple network architecture of this model limited its capacity for extracting deep image features. Ma et al. **[22]** first introduced the idea of adversarial game into the field of image fusion and proposed the FusionGAN algorithm. Xing et al. [23] developed a network architecture integrating a Variational Autoencoder (VAE) compression framework, achieving multi-channel fusion alongside a higher compression ratio. This approach not only balances the fusion results but also improves the training stability of the GAN. The image fusion algorithm based on Transformer has become an important research direction in the fields of

image processing and multimodal fusion. Shi et al. [24] balanced the color distribution in fused images by designing a global-local dual adversarial loss and further eliminated color interference using a dedicated color loss function. Yao et al. [25] enhanced colors in low-light regions, addressed excessive noise through data synthesis and tailored loss functions, and significantly improved model fusion efficiency.This algorithm not only improves the quality of image fusion but also enhances the generalization performance of the algorithm.

To sum up, although traditional image fusion algorithms achieve image fusion through mathematical transformation and artificially designed rules, reducing the requirements for hardware to a certain extent, their limitations are becoming increasingly obvious due to the influence of image registration and image noise. Deep learning, leveraging its advantages in adaptive feature extraction and processing efficiency, has emerged as a prominent research focus in the image fusion field. However, several challenging issues persist in existing deep learning-based methods that require urgent attention.

1) Inherent differences in scene information captured by infrared and visible sensors pose a challenge. The prevalent use of sequential convolutional layers for feature extraction often fails to adequately capture the complementary information from both modalities. This leads to insufficient perception of objects in salient regions and difficulties in simultaneously preserving global intensity distribution from infrared images and fine texture details from visible images.

2) Fused images are often prone to visual artifacts, which arise from both the inherent limitations of multi-source sensors and the instability of algorithm training. Consequently, despite achieving promising results on quantitative metrics, the perceptual quality of the fused image for human observers can be unsatisfactory, failing to meet the requirements for high-quality fusion.

3) Existing algorithms primarily rely on loss functions to enforce consistency of multi-source features in the fused image. However, in practical scenarios, depending on the conditions, visible images may sometimes reveal more distinct target features, while infrared images might occasionally provide clearer texture details. Such important, albeit secondary, information is often overlooked during the fusion process.

To tackle the aforementioned issues, this paper proposes a novel infrared and visible image fusion algorithm named DHAFGan, which integrates Shallow-Deep Feature Extraction and a Dual-channel Hybrid Attention mechanism. Firstly, a Shallow-Deep Feature Extraction (SDFE) module is designed to enable simultaneous learning of low-level details and deep semantic information through multi-receptive field processing. Secondly, a Dual-channel Hybrid Attention Fusion Module (DCAFM) is developed. This module decomposes features along spatial and channel dimensions for hierarchical fusion, facilitating the mining of important secondary information from the source images. Furthermore, a dual-discriminator architecture, guided by primary and secondary feature loss functions, is employed to enhance the complementarity of heterogeneous image information. Finally, Comprehensive experiments verify that the proposed DHAFGan algorithm generates fused images that are visually natural, rich in detail, and effectively preserve both primary and secondary information from the source images.

The main contributions of this study are summarized as follows:

1) We design a novel Shallow-Deep Feature Extraction (SDFE) module that enhances the perception of target information in salient regions. This leads to more abundant and accurate information representation in key areas of the fused image, thereby facilitating improved performance in downstream applications like target recognition and detection.

2) The proposed method effectively addresses the suboptimal human perceptual quality often associated with traditional fusion algorithms. The generated fused images exhibit more natural and clearer visual effects with reduced artifacts, thereby meeting the demands for high-quality visual perception and broadening the application scope of fused images in vision-related tasks.

3) We propose a Dual-channel Hybrid Attention Fusion Module (DCAFM) that enables the fused image to fully utilize important secondary information from less salient areas of the source images. This includes unique textures and details from either modality that may be prominent under specific conditions. This not only enriches the informational content of the fused result but also enhances its adaptability and robustness in complex and varying scenes.

4) We introduce a dual-discriminator adversarial training framework, optimized with primary and secondary feature loss functions. This design enhances the complementarity of heterogeneous image information. This ensures that the fused image retains critical source information while achieving a better balance of contributions from different modalities. Consequently, it generates high-quality, information-complete fused images, providing a more reliable foundation for subsequent image analysis and processing tasks.

2. Related Work

2.1. Overall framework of the algorithm

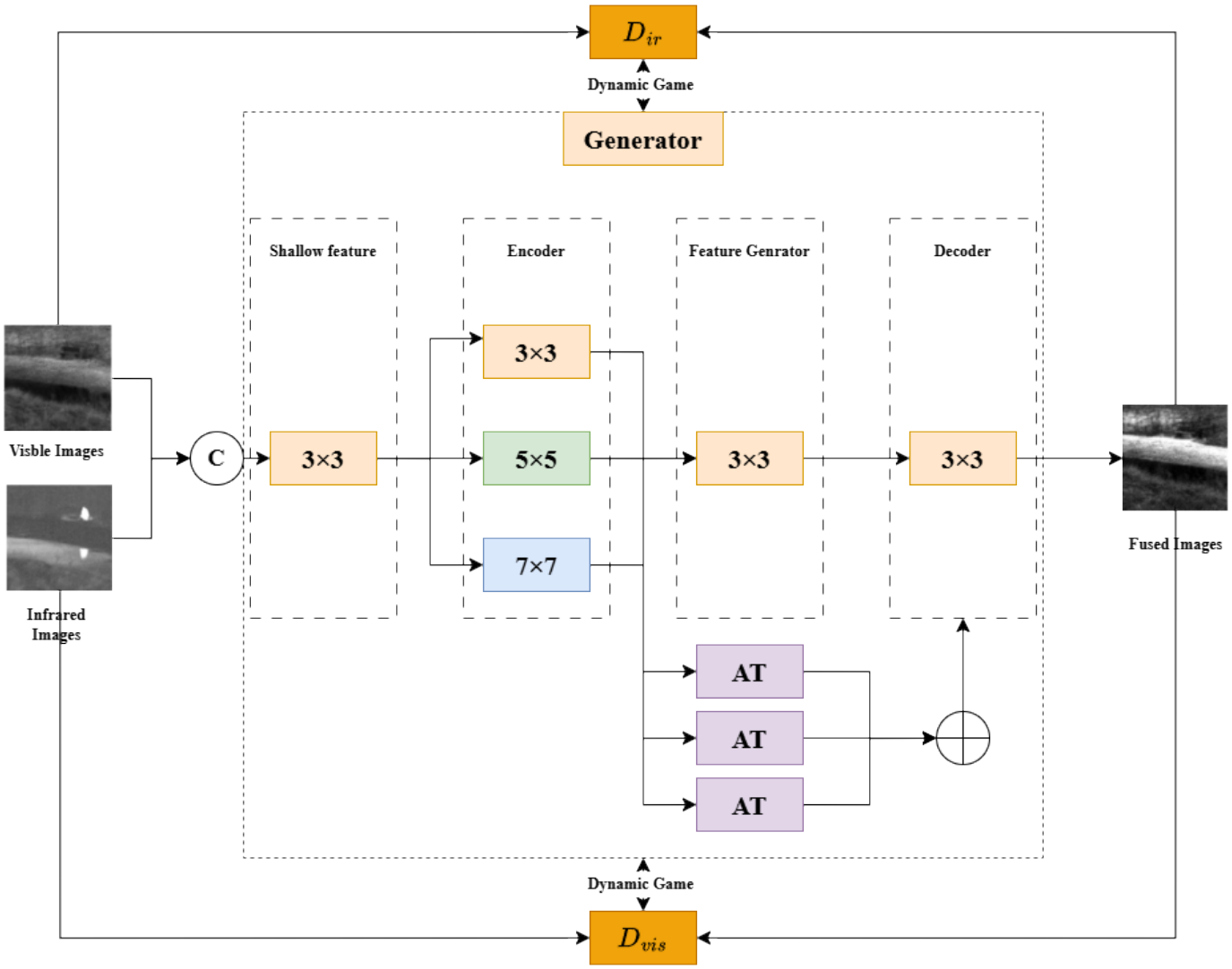

Fig.1. DHAFGan algorithm overall frame diagram

As shown in **Fig.1,** the core network framework of the proposed DHAFGan algorithm comprises a Generator and dual discriminators (D_{ir}, D_{vi}). Among them, the generator mainly includes the shallow-deep feature extraction module, the dual-channel hybrid attention fusion module and the decoder. The generator operates in an end-to-end manner. It leverages the complementary representations of infrared and visible modalities for the same scene to map the input image pairs into a fused feature representation. Furthermore, this paper adopts the image cascade preprocessing strategy, that is, the dual-modal images are concatenated and then fed into the encoder. This design enables the network to have dual-modal perception capabilities from the initial stage. This enables the generated images to retain fundamental infrared intensity characteristics and visible light gradient features even in the absence of the discriminator's constraints. Meanwhile, multi-receptive field deep feature extraction was constructed. This mechanism employs three parallel convolutional branches with kernel sizes of 3×3, 5×5, and 7×7 to simultaneously extract multi-scale deep features. The features from these heterogeneous receptive fields are first enhanced and then cascaded and integrated before being passed to the feature fusion module for multi-scale fusion. Finally, a fused image with dual-modal complementary characteristics is reconstructed by the decoder.

In this paper, a dual-channel hybrid attention fusion module is also constructed in the generator network, aiming to achieve the directional enhancement of single-source modal features based on the selective focusing characteristics of the attention mechanism. Specifically, in view of the characteristic that infrared images focus on the perception of intensity targets and the feature that visible light images emphasize the representation of gradient textures, the spatial-channel joint attention framework is constructed respectively. The multi-scale deep features extracted by three heterogeneous receptive field channels are processed in parallel. This process selectively enhances salient feature information while suppressing redundant components in both the spatial and channel dimensions. In the decoding stage, a hierarchical fusion strategy integrates the attention weights derived from different receptive field scales. This cross-scale integration ensures efficient feature transfer while mitigating information loss. Furthermore, an adversarial game architecture is established between the generator and the dual discriminators. Specifically,

the infrared discriminator (D_{ir}) ensures the fused image inherits the radiation characteristics of the infrared source through pixel-level intensity constraints. Conversely, the visible light discriminator (D_{vi}) enforces the preservation of fine texture details from the visible source through texture fidelity constraints. The adversarial training reaches an equilibrium when neither discriminator can reliably distinguish the generated image from its corresponding source image, indicating that the fusion result has met the desired objectives.

2.2 Generator Network Architecture

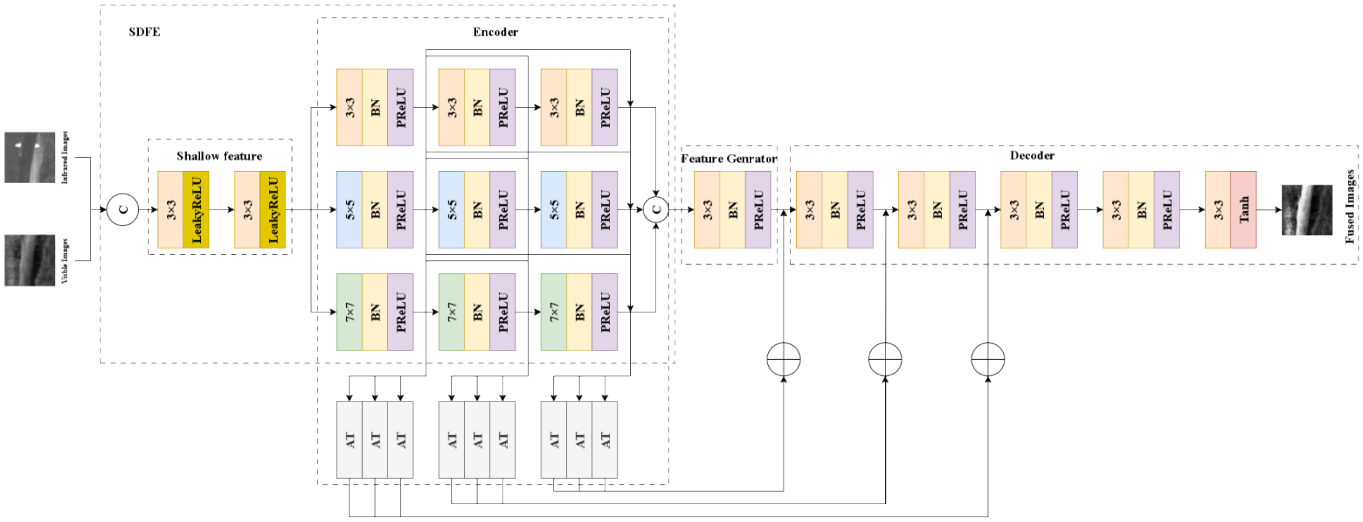

Fig. 2. Generator network structure diagram

As shown in **Fig. 2**, the proposed generator architecture sequentially consists of the Shallow-Deep Feature Extraction Module (SDFE), the Dual-channel Hybrid Attention Fusion Module (DCAFM), and the decoder. This cascaded architecture facilitates efficient inter-modality information fusion. The end-to-end design ensures computational efficiency while maximizing the retention of contrast information from infrared sources and texture details from visible sources. Consequently, it generates high-quality fused images that incorporate the advantages of both modalities.

2.2.1 ShAllow-Deep Feature Extraction Module (SDFE)

1) Shallow feature extraction

As shown in **Fig. 2**, the Shallow Feature Extraction (SFE) module serves as the foundational unit of the

network. It first constructs a primary feature representation of the input image by stacking convolutional layers. This module employs a convolutional network built with two 3×3 kernels, each followed by a LeakyReLU activation function (stride=1). This design effectively captures the basic semantic information present in the image. Furthermore, by performing spatial filtering operations on the input source image information using convolution kernels, low-level visual features such as edges and textures can be accurately extracted and mapped to the high-dimensional feature space to enhance the feature expression ability. This extraction strategy not only generates a preliminary abstract representation of the input data but also lays the groundwork for subsequent deep feature fusion. The shallow feature mapping process is defined as follows:

$$\left\{F_{SF}^{1},F_{SF}^{2}\right\} = H_{SE}(I_1),H_{SE}(I_2)(1)$$

In the formula, F_{SF}^{1} andF_{SF}^{2} are the dual-modal shallow feature representations extracted from the visible light image I_1 and the infrared image I_2; $H_{SE}(\cdot)$ is the feature extraction operation containing 3×3 convolution kernels and LeakyReLU. After the shallow feature extraction is completed, the obtained feature maps F_{SF}^{1} and F_{SF}^{2} will be input into the deep feature extraction module of the multi-receptive field for further processing. This module realizes the feature aggregation of local receptive fields through the cascading convolutional neural network architecture and the sliding window mechanism. Firstly, each convolutional kernel performs the weighted summation operation of the local region on the feature map, and introduces feature transformation through the nonlinear activation function, thereby constructing a deep feature representation with spatial invariance and hierarchical expression ability. Enhance the model's perception ability of multi-scale features.

2) Multi-receptive field deep feature extraction encoder

The performance of an image fusion algorithm hinges on the design of an efficient encoder architecture capable of accurately extracting core features from the source images and achieving comprehensive feature representation. Existing studies **[26]** have shown that the feature extraction capability of the encoder directly determines the upper bound of fused image quality. Conventional deep learning methods often

enhance multi-scale feature extraction by simply increasing network depth or channel capacity. Although this can expand the receptive field and capture deeper semantics, it invariably leads to an exponential growth in parameters, increasing the risk of unstable training (e.g., vanishing gradients). Moreover, information attenuation commonly occurs during cross-layer feature transfer, ultimately degrading fusion results. Therefore, it is necessary to balance the characterization ability and computational efficiency of the encoder.

To enhance the integrity of the model's feature extraction from the source image and expand the coverage of the receptive field, as shown in **Fig.2**, this paper constructs a multi-scale feature extraction module containing three types of convolution kernels: 3×3, 5×5, and 7×7. However, increasing the receptive field to improve feature extraction accuracy also leads to an exponential growth in the number of parameters. To this end, this paper draws on the network optimization strategy of Inception V3**[27]** and adopts a composite convolution kernel alternative scheme: decomposing a single 5×5 convolution into two serialized 3×3 convolution layers, and decomposing a 7×7 convolution into a cascading structure of three 3×3 convolution layers. This decomposition method enables the model to reduce the number of model parameters by approximately 61% (5×5→2×3×3, 7×7→3×3×3) while maintaining the equivalent receptive field, and significantly reduces the computational complexity of the model. Furthermore, a parameterized PRelu activation function is introduced in the convolution module. By introducing a negative response interval, the nonlinear expression ability of the network is enhanced, thereby improving the discriminative performance of the model.

The multi-receptive field feature extraction module designed in this paper adopts a unified architecture design. Each receptive field branch consists of three sequentially connected convolutional blocks. Each block contains a convolutional layer, a Batch Normalization (BN) layer, and a PReLU activation layer. To ensure the consistency of feature representation, the channel dimension of all convolutional layers is 32, the fixed step size is 1, and the spatial resolution of the feature map is maintained through Zero Padding, thereby avoiding the loss of spatial information during the feature extraction process. Furthermore, this

module introduces the dense connection mechanism of DenseNet [28]. By establishing feedforward connections between each layer and all previous layers, it achieves an exponential growth of the feature propagation path. This architectural design enables the network to capture richer semantic information, effectively extract the more complementary multi-scale feature representations in the source images, and provide high-quality feature input images for the subsequent fusion stage.

2.2.2 Feature Generator Architecture

The feature generator, as a key module of deep feature fusion, its core function lies in the refined processing of cascaded multi-receptive field deep features, and significantly improves the accuracy of feature representation through feature reconstruction and enhancement. This module incorporates three core components: a 3×3 convolutional layer (stride=1), a Batch Normalization (BN) layer, and the PReLU activation function. This lightweight architecture ensures computational efficiency while enabling in-depth mining of multi-scale features and optimizing feature fidelity.

2.2.3 Decoder Architecture

As the final part of generating the fused image, the decoder's input image comes from the multi-scale feature output of the feature generator, aiming to generate a fully information-complete fused image by fusing multimodal deep features. The decoder employs a five-layer progressive convolutional architecture: The first block consists of a 3×3 convolutional layer (32 channels) followed by PReLU. The second to fourth blocks each contain a 3×3 convolution (with channels set to 32, 32, and 16, respectively), a BN layer, and a PReLU activation. The final block uses a 3×3 convolutional layer (1 channel) with a Tanh activation function for output normalization. In particular, the first three convolutional layers establish a direct association with the multi-receptive field deep attention map in the encoder through skip connections. This design effectively mitigates semantic information attenuation caused by deep convolution and enhances cross-layer feature fusion capability. Furthermore, the consistent use of the PReLU activation function throughout the decoder leverages its adaptive parameter learning mechanism, which not only improves model convergence but also enhances the network's adaptability to complex

scenarios.

2.2.4 Dual-Channel Hybrid Attention Fusion Module (DCAFM)

The multi-attention mechanism, as the core technology of visual saliency detection, has shown extensive application value in the field of computer vision. Given that infrared and visible light images represent different feature dimensions of the same scene as typical multimodal data, this paper constructs a dual-channel hybrid attention fusion module, as shown in **Fig.3** This module synchronously captures salient feature regions from both modalities via its dual-channel attention mechanism. And based on the modal-specific weight allocation strategy, the differentiated representations of the same scene features in different modalities are weighted and enhanced, so that the feature maps generated by the convolutional neural network simultaneously contain the semantic information of the channel dimension and the position information of the spatial dimension. The Attention features from both dimensions carry critical discriminative information. Furthermore, the weight matrices of spatial attention and channel attention are calculated in parallel, and the hierarchical fusion of multi-scale features is carried out based on the receptive field hierarchy. The designed deep attention fusion module adopts a cascading architecture and, through a progressive feature fusion mechanism, enhances the local detail representation while retaining the global semantic association.

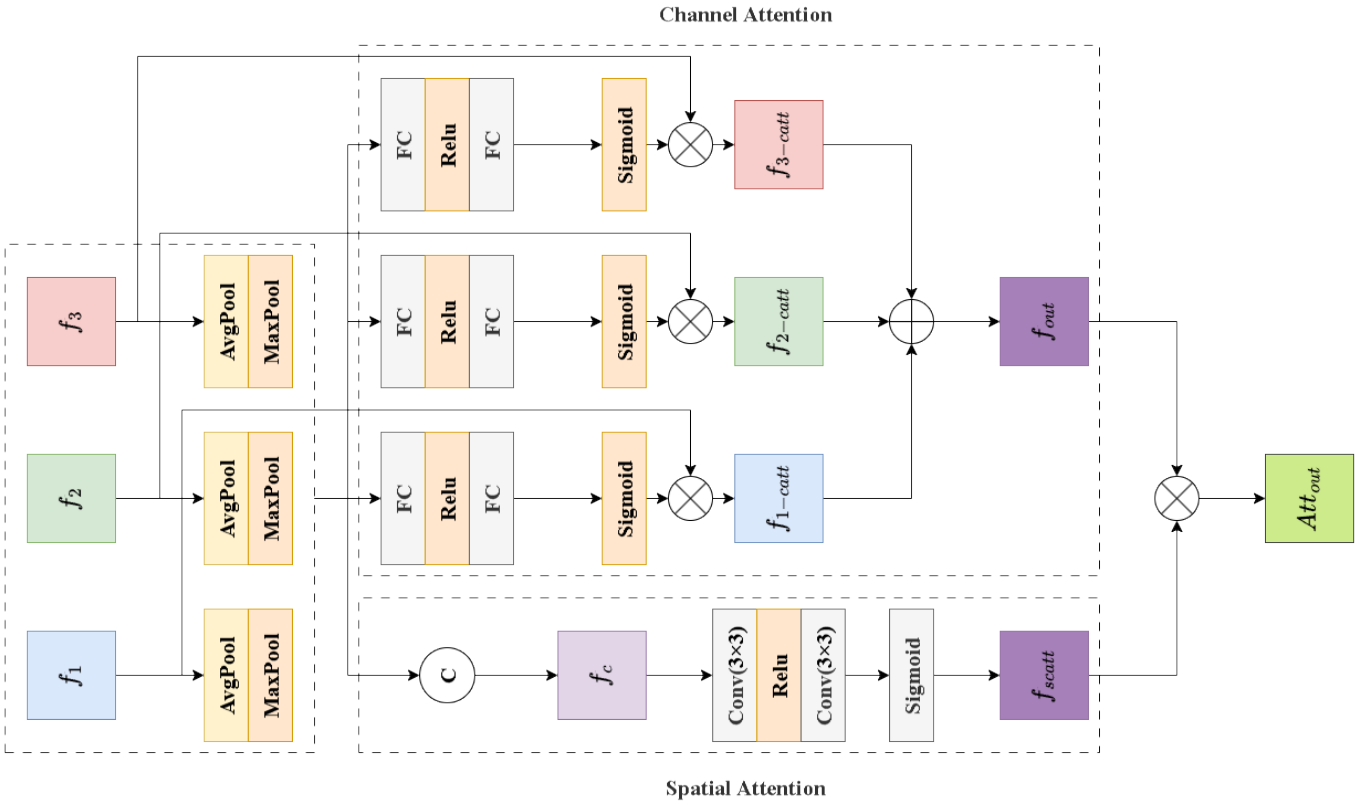

Fig. 3. Dual channel hybrid attention fusion module

1) Fusion of channel attention

First of all, according to the three characteristics of the reception field channel $f_1 \in \mathbb{R}^{H\times W\times C}$, $f_2 \in \mathbb{R}^{H\times W\times C}$ and $f_3 \in \mathbb{R}^{H\times W\times C}$, In this paper, Global Average Pooling (GAP) and Global Max Pooling (GMP) operations are implemented in parallel in the spatial dimension ($H \times W$) to generate three $1 \times 1 \times C$ feature vectors with the channel dimension of C. Subsequently, the obtained feature vectors are subjected to nonlinear transformation through a two-layer fully connected network, and the ReLU activation function is introduced to enhance the feature expression ability. On this basis, the Sigmoid activation function is used to normalize the processed feature map to generate the channel attention weight matrix $W^c \in \mathbb{R}^{C\times 1\times 1}$. Finally, the weight matrix is fused with the original feature map through channel weighted summation to obtain the feature representation f_{out}^c with enhanced channel dimensions, which is defined as follows:

$$f_{out}^c = \sum_{i=1}^{3} \sigma\left(D_2(D_1(avgp(f_i^c)))\right) \times f_i^c(2)$$

In the formula, $i = 1,2,3$, f_1^c, f_2^c and f_3^c are the channel features extracted by the convolution kernels with 3×3, 5×5 and 7×7 sensing fields, D_1 and D_2 are the two-layer fully connected operations, avgp represents the global average pooling operation, and $\sigma(\cdot)$ is the Sigmoid activation function. H, W and C are the height, width and channel dimension of the feature map.

2) The integration of spatial attention

First of all, according to the three characteristics of the reception field channel $f_1 \in \mathbb{R}^{H\times W\times C}$, $f_2 \in \mathbb{R}^{H\times W\times C}$ and $f_3 \in \mathbb{R}^{H\times W\times C}$, In this paper, Global Average Pooling (GAP) and Global Max Pooling (GMP) operations are implemented in parallel on the channel dimension to generate $H \times W \times 1$ feature maps with three spatial dimensions of $H \times W$. Subsequently, the three feature maps are cascaded along the channel dimension and feature transformation is carried out through a convolutional neural network composed of two layers of 3×3 convolutional kernels. Among them, the activation function ReLU is adopted to enhance the nonlinear expression ability of the model. Furthermore, the Sigmoid activation function is adopted to normalize the intermediate feature map, generating the spatial attention weight matrix $W^c \in \mathbb{R}^{H\times W\times 1}$. Finally, by weighted fusion of the spatial attention weight matrix and the channel attention fusion feature f_{out}^c, the deep attention feature map Att_{out}^c is obtained, which is defined as follows:

$$\mathrm{Att}_{out}^c = \sigma(Conv_2(Conv_1(C(avgp(f_i^c))))) \times f_{out}^c (3)$$

In the formula, $i = 1,2,3$, f_1^c, f_2^c and f_3^c are the channel features extracted by the convolution kernels with 3×3, 5×5 and 7×7 sensing fields respectively. $Conv_1 1$ and $Conv_2$ are two stacked convolution operation layers respectively, with the convolution kernel size being 3×3. avgp represents the global average pooling operation. $\sigma(\cdot)$ is the Sigmoid activation function, and H, W, and C represent the height, width, and channel dimension of the feature map respectively.

2.3 Discriminator Network Architecture

For the multimodal attribute fusion task of infrared and visible light image fusion, since the two types of source images have both modal differences and feature complementarity, this section constructs a dual discriminator architecture - infrared discriminator (D_{ir}) and visible light discriminator (D_{vis}). This

architecture is designed to maintain a balance between multimodal attributes through joint optimization, while accurately identifying the distribution discrepancies between the generated fused image and the corresponding modal source images. Specifically, the D_{ir} discriminator focuses on constralizing the retention ability of the fusion result for the intensity characteristics of the infrared mode, while the D_{vis} discriminator enhances the characterization ability of the detailed texture of the visible light mode. This differentiated constraint strategy effectively mitigates inter-modal information conflict and facilitates the effective integration of complementary features. During the network training process, it is necessary to strictly ensure the dynamic balance between the generator and the dual discriminator. When the training efficiency of any one of the three networks - the generator (G), the infrared discriminator (D_{ir}), and the visible light discriminator (D_{vis})-is significantly improved, it will lead to the suppression of the optimization processes of the other two networks. The dominant network would then impose its specific modal constraints more strongly, biasing the fusion result towards its modality and thereby weakening the influence of the other networks. Such imbalance directly disrupts the information retention mechanism in the fused image, ultimately degrading its overall performance. Therefore, establishing an effective network balance strategy is crucial for ensuring the collaborative optimization of multimodal features.

The proposed DHAFGan framework addresses this balance through a combination of its architectural design and carefully formulated loss functions. Since the discriminator, as a binary classifier, has significantly lower structural complexity than the generator, its core function lies in accurately determining the true and false attributes of the input image. Consequently, we adopt a symmetrical Siamese network architecture to construct the dual discriminators. As shown in **Fig. 4**, where the infrared discriminator and the visible light discriminator have the same network architecture but independent parameters. Each discriminator contains four cascades of convolutional blocks: Firstly, a single convolutional layer is used in combination with the LeakyReLU activation function to construct the first convolutional block; Secondly, a composite structure of convolutional layers, batch normalization (BN), and LeakyReLU is adopted to construct the second and third convolutional blocks; Finally, the fully connected layer and the Tanh

activation function are used to form the fourth convolutional block. The size of all convolution kernels is uniformly set to 3×3, and the step size is set to 1 to ensure that the size of the feature map decreases according to the step size. The channel dimension expands progressively through the network, set to 32, 64, and 128 in successive blocks, thereby establishing an effective feature abstraction hierarchy.

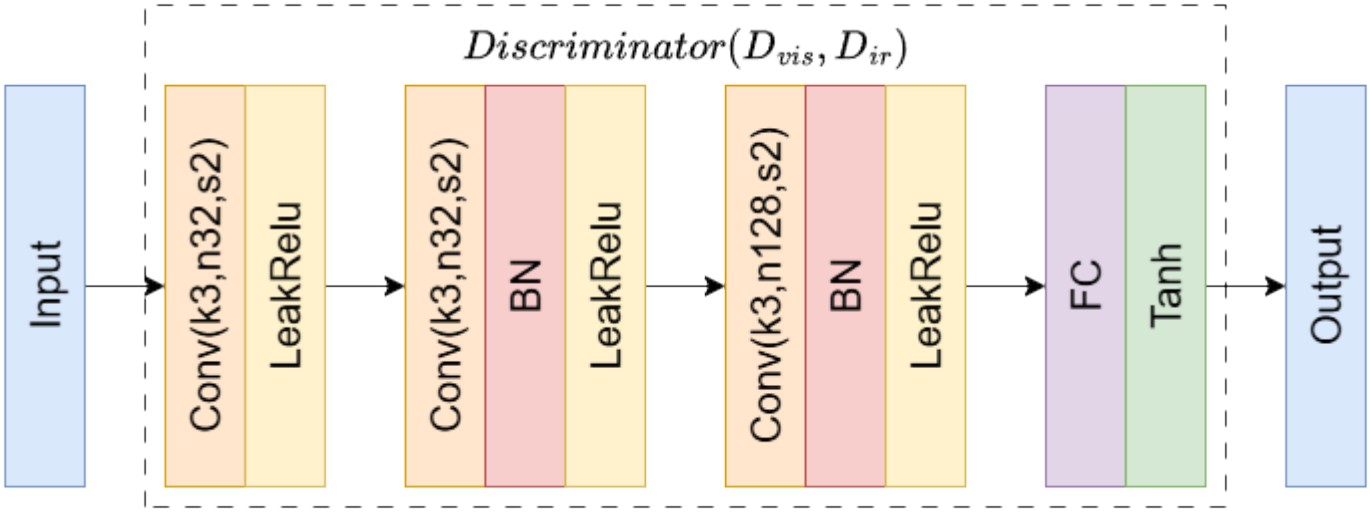

Fig.4. Network framework of discriminator

2.4 Loss Function

The loss function is pivotal for ensuring the dynamic balance between the generator and the discriminator. Through adversarial training, the generator and discriminators contend to balance feature retention. The generator must produce outputs whose data distribution aligns with that of the source images. Therefore, our loss function imposes constraints from two perspectives: spatial structural similarity and semantic content fidelity. Structurally, adversarial loss encourages the generated image's distribution to match that of the real source images. In terms of content, multi-scale feature loss is introduced to preserve key semantic information from the sources. This dual-constraint mechanism not only enhances the realism of the fused image but also effectively 'deceives' the discriminators, making it difficult to distinguish the generated result from real sources, thereby accelerating adversarial training convergence. The total loss of DHAFGan in this paper consists of two parts: the discrimination loss $\mathcal{L}_G$ and the content loss $\mathcal{L}_D$, which are defined as follows:

$$\begin{cases} min\mathcal{L}_G = \mathcal{L}_{adv} + \lambda\mathcal{L}_c \\ \mathcal{L}_c = \xi_1\mathcal{L}_{ssim} + \xi_2\mathcal{L}_{text} + \xi_3\mathcal{L}_{grad} \\ min\mathcal{L}_D = \begin{cases} \mathcal{L}_{D_{ir}} \\ \mathcal{L}_{D_{vis}} \end{cases} \end{cases} (5)$$

In the formula, $\mathcal{L}_G$ is the generator loss; $\mathcal{L}_{adv}$ is the generator adversarial loss; $\mathcal{L}_c$ is the feature loss; λ,ξ_1, ξ_2,ξ_3 are hyperparameters; $\mathcal{L}_{ssim}$ is the structural similarity loss; $\mathcal{L}_{text}$ is the texture loss; $\mathcal{L}_{grad}$ is the gradient loss; $\mathcal{L}_D$ is the discriminator loss; $\mathcal{L}_{D_{ir}}$ is the infrared discriminator loss. Loss of $\mathcal{L}_{D_{vis}}$ visible light discriminator.

2.4.1 Generator adversarial loss $\mathcal{L}_G$

This loss includes the adversarial loss component based on the infrared discriminator, which is used to constrain the authenticity of the fusion result in the infrared feature space, and the adversarial loss component based on the visible light discriminator, aiming to ensure the visual fidelity of the generated image in the visible light mode. This dual-branch adversarial mechanism facilitates collaborative optimization across the multimodal feature space via a strategy of differentiated constraints. It ensures that the fused image accurately represents infrared target features while fully retaining visible light scene details. It is defined as follows:

$$\mathcal{L}_{adv} = -E_{I_f \sim P_G}\left[D_{ir}(I_f)\right] - E_{I_f \sim P_G}\left[D_{vis}(I_f)\right] (5)$$

In the formula, I_f is the sample of the fused image of the generator; P_G is the data distribution of the fused image; D_{ir} and D_{vis} are the infrared and visible light source images respectively.

The structural similarity loss $\mathcal{L}_{ssim}$ is defined as follows:

$$\mathcal{L}_{ssim} = \theta_1\left(1 - ssim(I_f,I_1)\right) + \theta_2\left(1 - ssim(I_f,I_2)\right) (6)$$

In the formula, θ_1 and θ_2 are hyperparameters, both with a value of 0.5; I_1, I_2 and $I_f$are the infrared image, visible light image, and fused image respectively; $ssim(\cdot)$ is the structural similarity operation.

The texture loss $\mathcal{L}_{text}$ is defined as follows:

$$\mathcal{L}_{text} = \frac{\||\nabla I_f| - max(|\nabla I_1|,|\nabla I_2|)\|}{HW} (7)$$

In the formula, ∇ is the Sobel gradient operator, used to calculate texture information, $|\cdot|$ is the absolute

value of the calculation, $\|\cdot\|_1$ is the 1-norm of the matrix, and H and W are the length and width of the image respectively.

The gradient loss $\mathcal{L}_{grad}$ is defined as follows:

$$\begin{aligned}\mathcal{L}_{grad} &= \mathcal{L}_{grad_{main}} + \mathcal{L}_{grad_{aux}} \\ &= \delta_1\|I_f - I_{ir}\|_F^2 + \delta_2\|\nabla I_f - \nabla I_{vis}\|_F^2 \\ &+ \delta_3\|I_f - I_{vis}\|_F^2 + \delta_4\|\nabla I_f - \nabla I_{ir}\|_F^2\end{aligned} \quad (8)$$

In the formula, $\mathcal{L}_{grad_{main}}$ is the primary gradient loss, $\mathcal{L}_{grad_{aux}}$ is the secondary gradient loss, δ is the hyperparameter, I_f, I_{ir} and I_{vis} are the source image data sampling and source image data sampling respectively, and ∇ is the Laplacian operator, which is used to extract the edge information of the fused image. $\|\cdot\|_F^2$ is the L2 norm.

2.4.2 Discriminator loss $\mathcal{L}_D$

In this paper, a dual-discriminator architecture is adopted for design, and two independent optimization objectives, namely visible light discrimination loss and infrared discrimination loss, are constructed respectively. This dual-branch design, with its modality-specific constraints, enables the fused image to inherit distinct characteristics from each source: Dvis focuses on preserving high-frequency information like detailed textures, while Dir emphasizes maintaining contrast features such as target contours. Compared with the single discriminator architecture, the dual discriminator not only enhances the feature complementarity between modalities, but also realizes the efficient integration of cross-modal information, thereby significantly improving the representation ability of the fusion results in the multi-dimensional feature space. The loss function is defined as follows:

$$\begin{aligned}\mathcal{L}_{D_{ir}} &= -E_{x\sim P_{ir}}[D_{ir}(x)] + E_{I_f\sim P_G}\left[D_{ir}(I_f)\right] \\ &+ \phi_1 E_{\tilde{x}\sim penalty}\left[\|\nabla_{\tilde{x}} D_{ir}(\tilde{x})\|_2 - 1\right]^2\end{aligned} \quad (9)$$

$$\begin{aligned}\mathcal{L}_{D_{vis}} &= -E_{x\sim P_{vis}}[D_{vis}(x)] + E_{I_f\sim P_G}\left[D_{vis}(I_f)\right] \\ &+ \phi_2 E_{\tilde{x}\sim penalty}\left[\|\nabla_{\tilde{x}} D_{vis}(\tilde{x})\|_2 - 1\right]^2\end{aligned} \quad (10)$$

In the formula, P_{ir} and P_{vis} are the source data samples; P_G is the fused image sample; $\tilde{x}$ is the uniform sampling points in the continuous area formed by the real sample space and the generated sample space; ϕ_1

and ϕ_2 are the hyperparameters to ensure the balance of the loss function.

3. Experimental

3.1 Experimental Setup

All experiments were conducted on a computing platform equipped with an Ubuntu 18.04 operating system, an NVIDIA GeForce RTX 3060 GPU (12GB VRAM), and the PyTorch deep learning framework. The algorithm parameters are set as follows: $\delta_1 = 1$, $\delta_1 = 1$, $\delta_1 = 3$ and $\delta_1 = 0.2$, λ=ξ_1=ξ_2=9, the initial learning rate is 0.0001, the attenuation coefficient is set to 0.9, the epoch is set to 100, and the batchsize is set to 8; Update the parameters using the Adam optimizer. Furthermore, to mitigate potential training instability caused by the discriminator becoming too proficient too quickly, we employed a training schedule where the generator and discriminators were updated at a frequency ratio of 2:4 (generator : discriminators).To verify the performance of the algorithm, this paper selects the DroneVehicle dataset for experiments. The DroneVehicle dataset is a large-scale public benchmark containing paired infrared and visible images captured by Unmanned Aerial Vehicles (UAVs). It comprises 56,878 aligned infrared and visible image pairs, covering diverse road scenes (e.g., highways, communities, residential areas) and environmental conditions (e.g., daytime, nighttime). The imagery contains various vehicle categories, including vans, trucks, and hazardous chemical transport vehicles. The original images are surrounded by a 100-pixel white border, which we removed in a pre-processing step prior to training. **Fig.5** shows some image pairs of the DroneVehicle dataset. In the testing phase, 30 sets of images from the DroneVehicle dataset were used to form the test set, while the remaining image pairs were all used for model training.

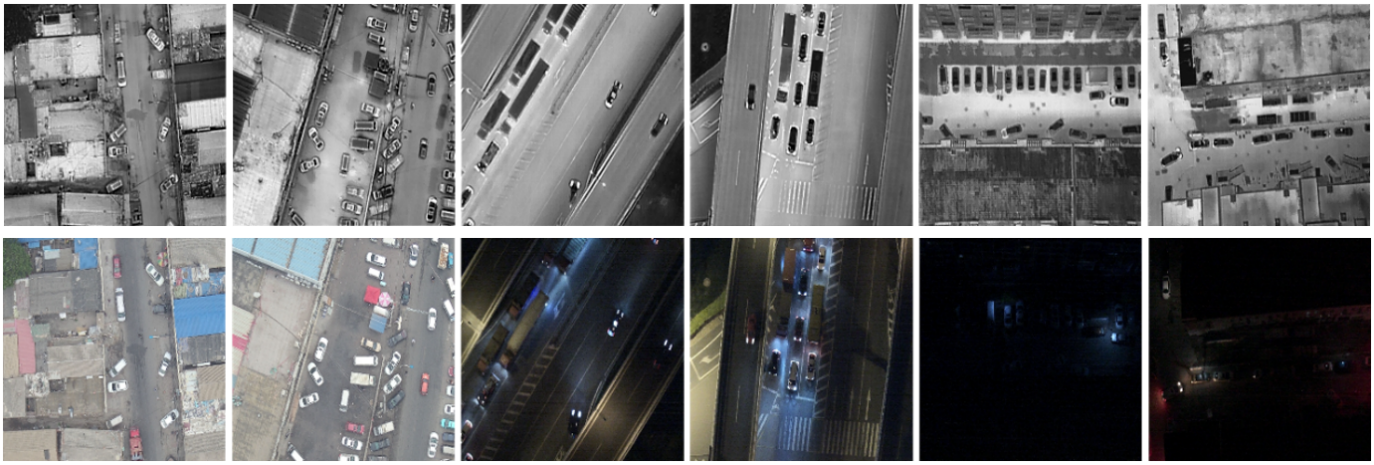

Fig. 5. Some typical image pairs in the DroneVehicle dataset

3.2 Evaluation index

This paper mainly evaluates the fusion results from both subjective and objective aspects. Subjective evaluation involves human observers assessing the fused images based on criteria such as target distinctness, overall clarity, richness of texture details, and visual naturalness. The overall quality is then rated using a qualitative scale (e.g., "excellent," "good," "fair," "poor"). Different from subjective evaluation methods, objective evaluation methods mainly quantitatively evaluate image quality through statistical calculations of information such as the gradient, intensity, and contrast of the target object in the fused image. Since a ground-truth fused image is unavailable for real-world fusion tasks, objective evaluation relies on the characteristics of the source images. We adopt several widely-used metrics: The Average Gradient (AG) **[29]** measures the ability of the fused image to preserve detailed texture information, which is prominent in visible images. The Standard Deviation (SD)**[30]** was adopted to measure the gray level and contrast of the salient regions in the fused image, and Mutual Information (MI)**Error! Reference source not found.** was used to determine whether the fused image evenly retains the salient features in the source image. Finally, the peak signal-to-noise ratio (PSNR)**[32]** was used to measure the difference between the fused image and the ideal image.

3.2.1 Average gradient (AG)

The average gradient measures the ability of the fused image to retain the texture detail information in the

source image by statistically fusing the gradient information in the horizontal and vertical directions of the image and then calculating the mean value. The larger its value is, the more abundant the texture details of the fused image are retained. It is defined as follows:

$$AG = \frac{1}{M \times W} \sum_{i=1}^{M-1} \sum_{j=1}^{W-1} \sqrt{\frac{1}{2}\left(f_i^2(i,j) + f_j^2(i,j)\right)} \quad (11)$$

In the formula, M and W are the height and width of the fused image; $f(i,j)$ is the gray value magnitude of the fused image at position; $f_i^2(i,j)$ is the gradient information of the fused image in the horizontal direction, and $f_j^2(i,j)$ is the gradient information of the fused image in the vertical direction.

3.2.2 Standard Deviation (SD)

The standard deviation represents the fluctuation between pixel values by statistically analyzing the contrast and the dispersion degree of distribution in the fused image. The larger its value is, the more obvious the contrast feature in the infrared part of the fused image is, and the clearer the detailed information in the visible light part is. It is defined as follows:

$$SD = \sqrt{\sum_{i=1}^{M} \sum_{j=1}^{W} (F(i,j) - \mu)^2} \quad (12)$$

In the formula, μ is the average gray value of the fused image, representing the overall brightness.

3.2.3 Mutual Information (MI)

Mutual information measures the degree of information sharing between the source image and the fused image by calculating the normalized histogram. The larger the value, the better the fused image retains the object information in the salient regions of the source image, and there is less secondary information loss in the non-salient regions. It is defined as follows:

$$MI(I,J) = \frac{1}{2}(MI_{\mathrm{A,F}} + MI_{\mathrm{B,F}}) = \frac{1}{2}\left(\sum_{i=1}^{L-1} \sum_{j=1}^{L-1} q_{A,F}(i,j) \bullet \log_2 \frac{q_{A,F}(i,j)}{q_A(i) q_F(j)} + \sum_{i=1}^{L-1} \sum_{j=1}^{L-1} q_{B,F}(i,j) \bullet \log_2 \frac{q_{B,F}(i,j)}{q_B(i) q_F(j)}\right) \quad (13)$$

In the formula, L is the gray scale number of the fused image; $MI_{\mathrm{A,F}}$ and $MI_{\mathrm{B,F}}$ are the normalized

calculation of the single-source image and the fused image respectively; $q_A(i)$, $q_B(i)$, and $q_F(j)$ are the normalized histogram distribution maps of the source image A, source image B, and the fused image F respectively.

3.2.4 Peak Signal-to-Noise Ratio (PSNR)

The peak signal-to-noise ratio is calculated as the ratio of the maximum pixel value of the fused image to the mean square of the pixel values between the fused image and the ideal image to measure the distortion between the source image and the fused result image. The larger the value, the less distortion of the fused image. It is defined as follows:

$$PSNR = 10 \cdot \log_{10}\left(\frac{MAX_I^2}{MSE}\right) (14)$$

$$MSE = \frac{1}{M \times W}\sum_{i=1}^{M}\sum_{j=1}^{W}[I(i,j) - K(i,j)]^2 (15)$$

In the formula, MSE is the mean square deviation of the overall pixel values between the source image and the fused image; MAX_I is the maximum possible pixel value of the fused image.

4. Analysis and Discussion

4.1 Ablation Experiment

This section designs three groups of experiments to verify the effectiveness of the module designed in this paper. The qualitative and quantitative results of the ablation study are presented in **Fig. 6** and **Table 1**, respectively. In Table 1, the best results are highlighted in bold. Firstly, experiments were conducted by replacing the shallow-deep feature extraction module (w/o M1) in the encoder with continuous ordinary convolutional blocks. The experimental results showed that key indicators such as SD, AG, MI and PSNR all presented a significant downward trend. This demonstrates that the multi-receptive field design in SDFE is crucial for effectively extracting contrast information of vehicle targets from infrared images while simultaneously preserving the texture details of road markings from visible images. The experimental results fully verify the effectiveness of the M1 module design. Secondly, when the dual-channel hybrid

attention fusion module (w/o M2) was removed, indicators such as SD, AG, MI and PSNR all decreased significantly. This phenomenon underscores the critical role of the dual-channel attention mechanism in enhancing target saliency and preserving structural information. These results confirm that the DCAFM (M2) successfully enhances salient feature information through its dual-channel attention mechanism, thereby proving the rationality and effectiveness of its design. In summary, the module designed in this paper can effectively improve the effect of fused images.

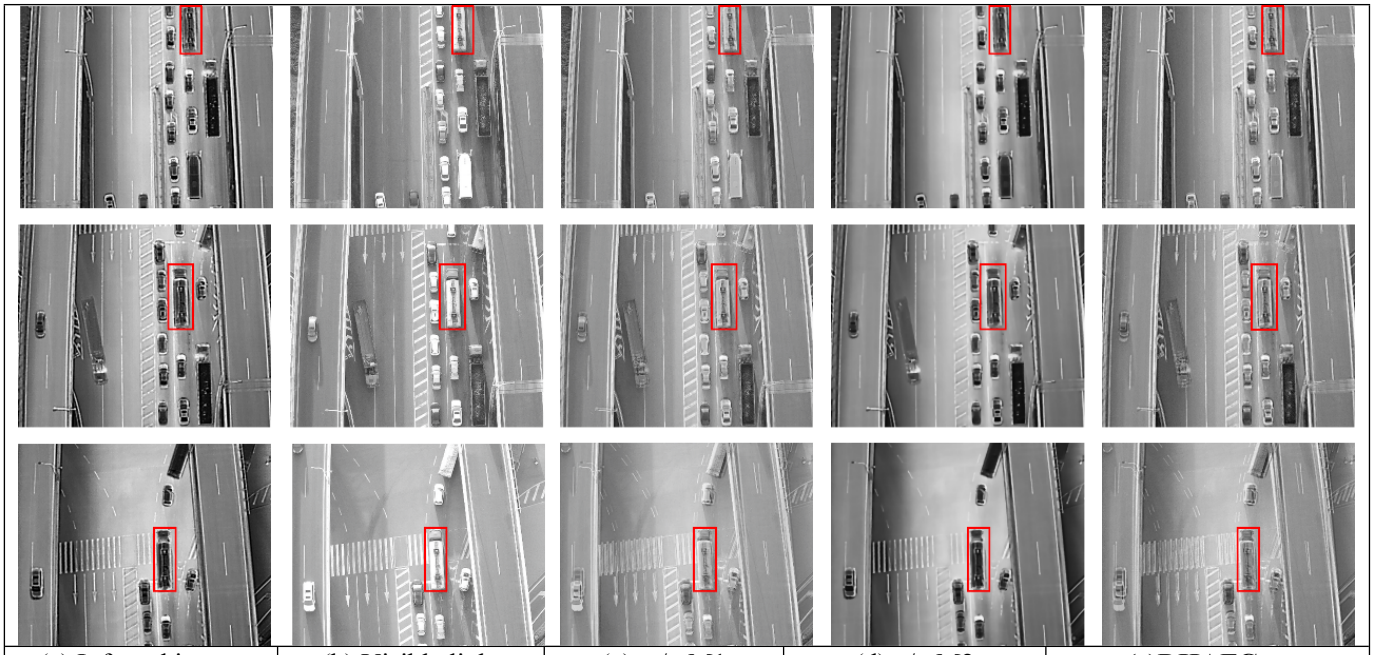

(a) Infrared image	(b) Visible light image	(c) w/o M1	(d)w/o M2	**(e)DHAFGan**

Fig. 6. Visualization result graph of the ablation experiment

Table 1. Quantitative Comparison Of Ablation Experiments

Method	SD	AG	MI	PSNR
w/o M1	7.5459	2.994	2.0543	62.735
w/o M2	8.4375	2.849	1.8572	60.254
DHAFGan	**9.3541**	**3.9854**	**2.4321**	**65.7852**

4.2 Comparative Experiment

4.2.1 Subjective qualitative evaluation

To systematically validate the performance advantages of the proposed algorithm, this section conducts a qualitative comparative analysis on three sets of representative fusion images selected from the test results on

the DroneVehicle dataset. The experimental results are presented in **Fig. 7**. The figure displays the fusion results of visible light images, infrared images, and eight different fusion algorithms, including Anisotropic Diffusion Fusion (ADF), Guided Filtering Fusion (GFF), Gradient Transfer Fusion (GTF), Ratio Pyramid (RP), Convolutional Neural Networks (CNN), Fusion Generative Adversarial Network (FusionGAN), Generative Adversarial Network with Multi-Class Constraints (GANMcC), and the proposed Dense Hybrid Attention Fusion Generative Adversarial Network (DHAFGan). As shown in **Fig. 7**, significant differences can be observed among the algorithms in terms of information retention, contrast enhancement, texture sharpness, and visual naturalness. The detailed analysis is as follows:

The fusion results of the ADF algorithm generally exhibit low overall brightness and insufficient image contrast, leading to poor distinction between targets and the background. Edge information in certain regions is blurred, particularly in details such as vehicle contours and road markings, resulting in an ineffective preservation of texture features from the visible light image.

Although the GFF algorithm can preserve the intensity information of the infrared image to some extent, the fusion images exhibit noticeable edge blurring. Texture information of vehicle targets is almost entirely lost, and background details are poorly represented, resulting in an overly smooth overall visual effect lacking in layering.

The GTF algorithm demonstrates prominent performance in enhancing target saliency and effectively preserves intensity information from the infrared image. However, excessive sharpening of moving vehicles leads to halo effects and artifacts in certain areas, causing visual distortion and compromising the naturalness of the image.

The fusion results of the RP algorithm achieve a relatively balanced performance in overall contrast and brightness. However, it still falls short in preserving detailed textures, with over-smoothing observed in certain regions, particularly in road textures and vehicle contours, leading to noticeable information loss.

Compared with traditional methods, the CNN algorithm performs better in balancing information, effectively retaining texture details from the visible light image and intensity information from the infrared image. The

fusion results are visually natural with high edge sharpness, though slight overexposure occurs in some highlight regions.

The FusionGAN algorithm preserves target intensity information from the infrared image relatively well but inadequately retains texture details from the visible light image, resulting in blurring and artifacts in some areas. The overall visual effect is somewhat dark, and the visual naturalness requires improvement.

The GANMcC algorithm exhibits moderate performance in integrating multi-modal information. The fusion images suffer from severe loss of background texture details and information loss in certain target regions, leading to poor overall visual quality and failing to meet the requirements of high-quality image fusion.

Compared with the aforementioned seven algorithms, the proposed DHAFGan algorithm demonstrates significant advantages in subjective visual performance. Specifically, DHAFGan completely preserves the structural features of the iron framework of occluded vehicles from the visible light image while effectively extracting and integrating salient target information from the infrared image, achieving a balanced representation of multi-modal features. The fusion results exhibit high visual similarity to the source images, without noticeable distortion, artifacts, or noise interference. The overall image brightness is moderate, and the contrast is natural, aligning well with human visual perception. In detailed regions such as road markings, vehicle contours, and background buildings, DHAFGan maintains high sharpness and texture integrity, effectively avoiding issues such as excessive sharpening and information loss commonly observed in traditional methods.

In summary, from a subjective visual perspective, the fused images generated by the DHAFGan algorithm achieve a high degree of consistency in apparent quality with visible light images while fully retaining the salient target information from infrared images. The algorithm significantly outperforms the other seven comparative algorithms in terms of information retention, visual naturalness, and texture sharpness, thereby fully validating its superior performance in multi-modal image fusion tasks.

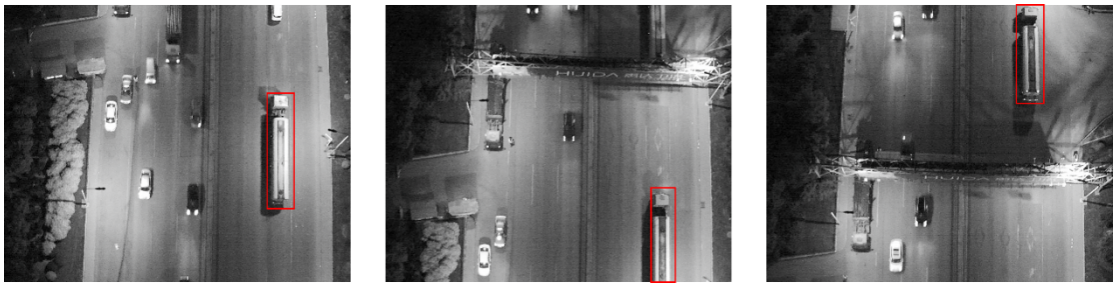

（a）Visible image

（b）Infrared image

（c）ADF

（d）GFF

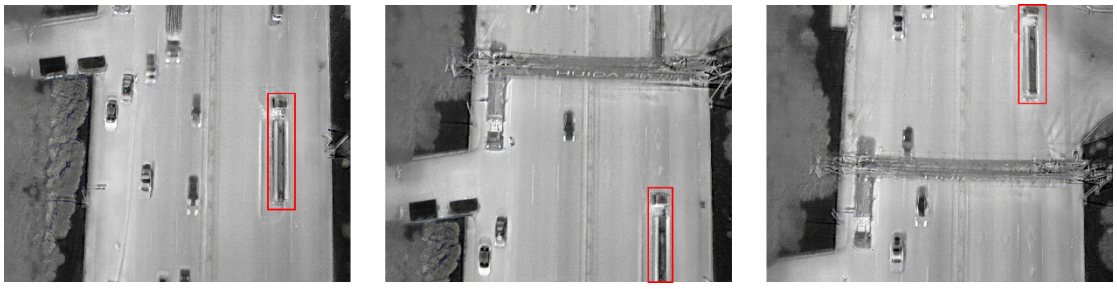

（e）GTF

（f）RP

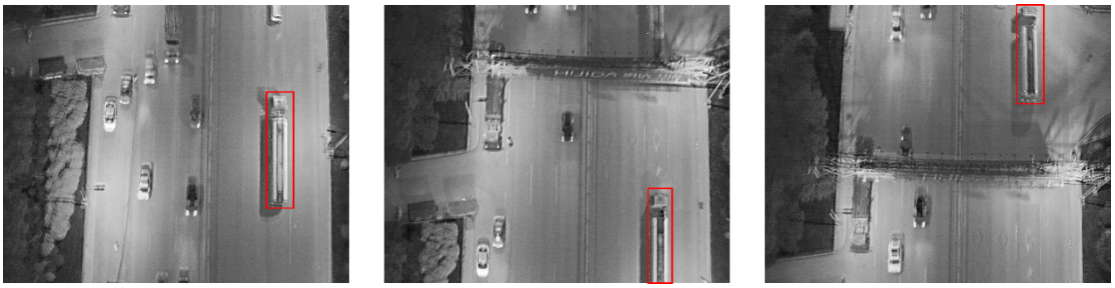

（g）CNN

（h）FusionGAN

（i）GANMcC

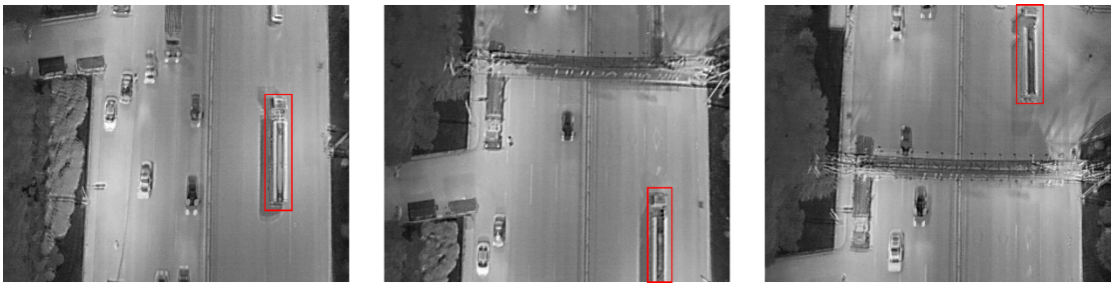

（j）DHAFGan

Fig.7. A comparison chart of the fusion results of the DroneVehicle dataset

4.2.2 Objective quantitative evaluation

The experimental results are shown in **Table 2**. The DHAFGan algorithm proposed in this paper performs the best in the SD index, and its value is significantly better than that of other comparison algorithms, fully

verifying the significant advantage of this method in improving the contrast of fused images. This translates to outstanding visual performance in the fused images. In terms of the AG index, the DHAFGan algorithm ranks second, indicating that its fusion results have certain advantages in maintaining texture gradient information. DHAFGan also ranks first on the MI metric, with a quantitative result substantially higher than other methods. This proves its superior ability to retain feature information from both source modalities. Finally, DHAFGan attains the top PSNR value, indicating its effectiveness in suppressing image distortion and resulting in the lowest level of visual noise among all compared algorithms. In summary, the quantitative analysis reveals that DHAFGan demonstrates dominant performance across three key metrics (SD, MI, PSNR). It is only slightly outperformed by the RP method on the AG index. This overall performance profile thoroughly validates the comprehensive superiority of our proposed method for the multimodal image fusion task, particularly highlighting its significant advantages in preserving source information integrity and enhancing visual quality.

Table 2. Quantitative comparison results of multiple fusion algorithms in the dronevehicle dataset

	ADF	FusionGAN	GANMCC	GFF	GTF	CNN	RP	DHAFGan
SD	8.4684	8.1253	9.1548	8.4526	8.3261	8.7536	8.6951	**9.3541**
AG	2.9132	2.2356	1.8732	3.3561	2.5943	3.7634	**4.4125**	3.9854
MI	1.8536	2.1873	0.8941	2.1357	2.3148	1.8549	1.8261	**2.4321**
PSNR	65.4816	61.2894	62.6542	61.3781	62.9155	63.5732	65.4561	**65.7852**

Note：The bolded results are the optimal results, and the results underlined are the second-best results.

4.2.3 Comparison of computational efficiency

This section conducts a quantitative comparative analysis of the fusion efficiency based on the test data. The experimental results are shown in **Table 3**. Compared to other deep learning-based fusion algorithms, the computational efficiency of our DHAFGan is slightly lower than that of FusionGAN. This difference is primarily attributed to the increased model complexity introduced by the multi-receptive field feature extraction and dual-channel hybrid attention fusion modules. Although the improvement in the model network architecture will lead to a relative increase in computing time, it can be known through the comprehensive analysis of

subjective evaluation and objective indicators that this algorithm shows significant advantages in the quality of fused images. Therefore, the design strategy of trading a moderate increase in inference time for a substantial improvement in fusion quality is justified and holds practical value for applications where image quality is paramount.

Table 3. Comparison of the average fusion time of the algorithm

	ADF	**FusionGAN**	**GANMCC**	**GFF**	**GTF**	**CNN**	**RP**	**DHAFGan**
Dronevehicle Mean(s)	0.7892	**0.1918**	0.2717	1.0226	3.8966	<u>0.2638</u>	0.5627	0.5437

Note：The bolded results are the optimal results, and the results underlined are the second-best results.

5. Conclusion

This paper has addressed key limitations in existing image fusion algorithms, including inadequate perception of salient features, generated images that are inconsistent with human visual perception, and underutilization of important secondary information. To this end, we have proposed DHAFGan, a novel infrared and visible image fusion algorithm based on shallow-deep feature extraction and dual-channel hybrid attention. Firstly, The core of our framework features a hierarchical feature extraction module, which integrates a shallow feature extraction component with a deep multi-receptive field fusion unit. This design enables parallel processing of low-level detail features and cross-scale high-level semantics, achieving a more comprehensive capture of multimodal features. Secondly, a dual-channel hybrid attention fusion module (DCAFM) was designed to perform adaptive, modality-specific feature weighting for the infrared and visible light streams. By reinforcing critical information and suppressing redundant components, it ensures the precise extraction of modal features that contribute most significantly to the fusion result. Furthermore, a dual-discriminator adversarial training architecture was also constructed. This architecture facilitates the dual optimization of feature fidelity and visual consistency through adversarial training, ensuring the fused image retains source features while conforming to human visual characteristics.

Finally, primary and secondary feature loss functions were formulated. These losses model the complementarity between intensity and gradient features for infrared images, while emphasizing the correlation between gradient and intensity information for visible images. This differentiated constraint strategy fully exploits the potential complementary information inherent in the dual-modal data. The experimental results show that the fused images generated by the algorithm in this paper achieve better fusion effects in subjective visual expression and are superior to seven typical fusion algorithms in objective indicators such as AG, MI and PSNR. The primary limitation of the current work is the increased computational time resulting from the model's complexity, which affects its fusion efficiency. Therefore, our future work will focus on developing fusion algorithms that maintain high performance while significantly improving computational efficiency, potentially through network lightweighting or knowledge distillation techniques.

Data availability

The data that support the findings of this study are available from the corresponding author upon reasonable request.

CRediT authorship contribution statement

Qiong Hong: Supervision, Project administration, Formal analysis, Conceptualization. Zhonghua Xu: Writing - review & editing, Writing - original draft, Visualization, Software, Resources, Project administration, Methodology, Formal analysis, Data curation, Conceptualization. Dongli Qin: Writing - review & editing, Data curation. Yuhui Zheng: Methodology, Data curation. Hao Zhang: Funding acquisition, Methodology, Data curation.

Declaration of competing interest

The authors declare that they have no known competing financial interests or personal relationships that could have appeared to influence the work reported in this paper.

Acknowledgment

This work was supported by Ministry of Education Humanities and Social Sciences Research Program (23YJA790099)，and the National Natural Science Foundation of China (71874067) and the ‘Qing Lan Project’ of Jiangsu Province.

References

[1] Dogra, B. Goyal, S. Agrawal, From multi-scale decomposition to non-multi-scale decomposition methods: A comprehensive survey of image fusion techniques and its applications[J]. IEEE Access, 2017, 5: 16040-16067. https://doi.org/10.1109/access.2017.2735865

[2] Dong L, Wang J. Infrared and visible light image fusion via pixel mean shift and source image gradient[J]. Infrared Physics & Technology, 2024, 136: 104767. https://doi.org/10.1016/j.infrared.2023.104767

[3] Jin H, Jiao L, Liu F, et al. Fusion of infrared and visual images based on contrast pyramid directional filter banks using clonal selection optimizing[J]. Optical Engineering, 2008, 47(2): 027002-027002-8. https://doi.org/10.1117/1.2857417

[4] Zuo Y, Liu J, Bai G, et al. Airborne infrared and visible image fusion combined with region segmentation[J]. Sensors, 2017, 17(5): 1127. https://doi.org/10.3390/s17051127

[5] Meng F, Song M, Guo B, et al. Image fusion based on object region detection and non subsampled contourlet transform[J]. Computers & Electrical Engineering, 2017, 62: 375 383. https://doi.org/10.1016/j.compeleceng.2016.09.019

[6] Ma J, Zhou Z, Wang B, et al. Infrared and visible image fusion based on visual saliency map and weighted least square optimization[J]. Infrared Physics & Technology, 2017, 82: 8-17. https://doi.org/

[7] Liu Y, Wang Z. Simultaneous image fusion and denoising with adaptive sparse representation[J]. IET Image Processing, 2015, 9(5): 347-357. https://doi.org/10.1016/j.infrared.2017.02.005

[8] Dong L, Wang J. Infrared and visible light image fusion via pixel mean shift and source image gradient[J]. Infrared Physics & Technology, 2024, 136: 104767. https://doi.org/10.1016/j.infrared.2023.104767

[9] Song C, Liu J, Wang C, et al. Rapid identification of adulterated rice based on data fusion of near-infrared spectroscopy and machine vision[J]. Journal of Food Measurement and Characterization, 2024, 18(5): 3881-3892. https://doi.org/10.1007/s11694-024-02462-5

[10] Zhang X, Wang X, Yan C, et al. EV-fusion: A novel infrared and low-light color visible image fusion network integrating unsupervised visible image enhancement[J]. IEEE Sensors Journal, 2024, 24(4): 4920-4934. https://doi.org/10.1109/jsen.2023.3346886

[11] Chen W, Miao L, Wang Y, et al. Infrared–Visible Image Fusion through Feature-Based Decomposition and Domain Normalization[J]. Remote Sensing, 2024, 16(6): 969. https://doi.org/10.3390/rs16060969

[12] Liu J, Wu G, Liu Z, et al. Infrared and visible image fusion: From data compatibility to task adaption[J]. IEEE Transactions on Pattern Analysis and Machine Intelligence, 2024. https://doi.org/

[13] Hou W, Liu X, Wang J, et al. Multispectral Land Surface Reflectance Reconstruction Based on Non-Negative Matrix Factorization: Bridging Spectral Resolution Gaps for GRASP TROPOMI BRDF Product in Visible[J]. Remote Sensing, 2025, 17(6): 1053. https://doi.org/10.1109/tpami.2024.3521416

[14] Wu B, Nie J, Wei W, et al. Adjustable Visible and Infrared Image Fusion[J]. IEEE Transactions on Circuits and Systems for Video Technology, 2024. https://doi.org/10.1109/tcsvt.2024.3449638

[15] Zhang B, Lu X, Pei H, et al. A fusion algorithm for infrared and visible images based on saliency analysis and non-subsampled Shearlet transform[J]. Infrared Physics & Technology, 2015, 73: 286-297. https://doi.org/10.1016/j.infrared.2015.10.004

[16] Zhang X, Ma Y, Fan F, et al. Infrared and visible image fusion via saliency analysis and local edge-preserving multi-scale decomposition[J]. JOSA A, 2017, 34(8): 1400-1410. https://doi.org/10.1364/josaa.34.001400

[17] Huang Y, Gao K, Gong C, et al. Infrared and visible image fusion with the target marked based on multi-resolution visual attention mechanisms[C], Chinese Society for Optical Engineering Conferences. Chengdu: SPIE, 2017: 775-782. https://doi.org/10.1117/12.2264771

[18] Li H, Wu X J. DenseFuse: A fusion approach to infrared and visible images[J]. IEEE Transactions on Image Processing, 2018, 28(5): 2614-2623. https://doi.org/10.1016/j.infrared.2023.104696

[19] Wang Z, Yang F, Sun J, et al. AITFuse: Infrared and visible image fusion via adaptive interactive transformer learning[J]. Knowledge-Based Systems, 2024, 299: 111949. https://doi.org/10.1016/j.knosys.2024.111949

[20] Liu Y, Chen X, Cheng J, et al. A medical image fusion method based on convolutional neural networks[C], IEEE conference, International conference on information fusion (Fusion). Piscataway: IEEE Computer Society, 2017: 1-7. https://doi.org/10.23919/icif.2017.8009769

[21] Xu H, Ma J. EMFusion: An unsupervised enhanced medical image fusion network[J]. Information Fusion, 2021, 76: 177-186. https://doi.org/10.1016/j.inffus.2021.06.001

[22] Ma J, Yu W, Liang P, et al. FusionGAN: A generative adversarial network for infrared and visible image fusion[J]. Information fusion, 2019, 48: 11-26. https://doi.org/10.1016/j.inffus.2018.09.004

[23] Xing M, Liu G, Tang H, et al. CFNet: An infrared and visible image compression fusion network[J]. Pattern Recognition, 2024, 156: 110774. https://doi.org/10.1016/j.patcog.2024.110774

[24] Shi Q, Xi Z, Li H. Nighttime visible and infrared image fusion based on adversarial learning[J]. Infrared Physics & Technology, 2025, 144: 105618. https://doi.org/10.1016/j.infrared.2024.105618

[25] Yao J, Zhao Y, Bu Y, et al. Color-aware fusion of nighttime infrared and visible images[J]. Engineering Applications of Artificial Intelligence, 2025, 139: 109521. https://doi.org/10.1016/j.engappai.2024.109521

[26] Szegedy C, Vanhoucke V, Ioffe S, et al. Rethinking the inception architecture for computer vision[C]. Proceedings of the IEEE Conference on Computer Vision and Pattern Recognition (ICCVPR), 2016: 2818-2826. https://doi.org/10.1109/cvpr.2016.308

[27] He K, Zhang X, Ren S, et al. Delving deep into rectifiers: Surpassing human-level performance on imagenet classification[C]. Proceedings of the IEEE International Conference on Computer vision (ICCV), 2015: 1026-1034. https://doi.org/10.1109/iccv.2015.123

[28] Huang G, Liu Z, Van Der Maaten L, et al. Densely connected convolutional networks[C]. Proceedings of the IEEE Conference on Computer Vision and Pattern Recognition (ICCVPR), 2017: 4700-4708. https://doi.org/10.1109/cvpr.2017.243

[29] Li Q, Yang S, Wu P, et al. HADF: A hybrid attention and dual-branch feature fusion method for infrared and visible image fusion[J]. Computer Vision and Image Understanding, 2025: 104557. https://doi.org/10.1016/j.cviu.2025.104557

[30] Shi W, Zhu C Q, Tian Y, et al. Wavelet-based image fusion and quality assessment[J]. International Journal of Applied Earth Observation and Geoinformation, 2005, 6(3-4): 241 251. https://doi.org/10.1016/j.jag.2004.10.010

[31] Dong L, Yang Q, Wu H, et al. High quality multi-spectral and panchromatic image fusion technologies based on curvelet transform[J]. Neurocomputing, 2015, 159: 268-274. https://doi.org/10.1016/j.neucom.2015.01.050

[32] Aslantas V, Bendes E. A new image quality metric for image fusion: The sum of the correlations of differences[J]. Aeu-international Journal of electronics and communications, 2015, 69(12): 1890-1896. https://doi.org/10.1016/j.aeue.2015.09.004